SUPPORTING INFORMATION

Fluorescence Anisotropy Decays and Microscale-Volume Viscometry Reveal the Compaction of Ribosome-Bound Nascent Proteins

Rachel B. Hutchinson[1], Xi Chen[1], Ningkun Zhou[1], and Silvia Cavagnero[1]

[1] Department of Chemistry, University of Wisconsin-Madison, Madison, WI 53706

SUPPLEMENTARY TEXT

Puromycin assay. A puromycin assay was used to verify that nascent proteins are ribosome-bound.[1, 2] For this assay, the RNC sample was split into two aliquots. Puromycin was added to one aliquot to reach a final puromycin concentration of 1 mM. This aliquot was incubated for 30 min at 37 °C. The two aliquots were analyzed with an SDS-PAGE gel as shown in Figure S1. The sample treated with puromycin shows a smaller molecular weight than the sample lacking puromycin, demonstrating that this nascent chain had been released from the ribosome, and confirming that the sample was ribosome-bound prior to the addition of puromycin. The puromycin treatment was performed on the samples employed for fluorescence measurements after completion of fluorescence and microscale-volume viscometry data collection.

Steady-state versus anisotropy-decay measurements. In steady-state fluorescence anisotropy, the excitation light source is continuous, and it has a constant intensity. The excitation time is considerably longer than the sample fluorescent lifetime, so the measured fluorescence anisotropy is averaged over time. Time-averaged anisotropy and rotational correlation time provide information about the average size and shape for the whole sample. However, steady-state methods cannot resolve independent rotational motions within the same molecule, each associated with a different rotational correlation time.

In contrast, fluorescence anisotropy decay measurements are based on a more complex excitation scheme. Pulsed excitation is used for time-domain anisotropy measurements and sinusoidally-modulated excitation amplitude is used for frequency-domain measurements. In both cases, changing the intensity of the excitation source enables determining fluorescence-anisotropy decays, as long as they take place within the fluorophore lifetime. Multiple fluorescence anisotropy decays occurring within the same sample lead to the detection of

multiple rotational correlation times provided that these times are (a) comparable to or shorter in duration than the fluorophore's fluorescent lifetime and (b) they significantly differ from each other, typically by at least a factor of five.

Time-dependent fluorescence anisotropy as a function of time is defined as

$$r(t) = \frac{(I_{\parallel}(t) - I_{\perp}(t))}{(I_{\parallel}(t) - 2I_{\perp}(t))} \quad . \tag{1}$$

For a spherical species with a single fluorescent lifetime τ_F and a global rotational correlation time τ_c, $I_{\parallel}(t)$ and $I_{\perp}(t)$ are

$$I_{\parallel}(t) = \left[\frac{1}{3} + \left(\frac{4}{15}\right) e^{-\frac{t}{\tau_c}} \frac{(3\cos^2\xi - 1)}{2}\right] e^{-\frac{t}{\tau_F}} \tag{2}$$

and

$$I_{\perp}(t) = \left[\frac{1}{3} - \left(\frac{2}{15}\right) e^{-\frac{t}{\tau_c}} \frac{(3\cos^2\xi - 1)}{2}\right] e^{-\frac{t}{\tau_F}} \quad . \tag{3}$$

Substitution of eqs 2 and 3 into eq 1 gives eq 4, which defines the time-dependent fluorescence anisotropy of a sample with a single rotational correlation time

$$r(t) = r_0 e^{-t/\tau_c} \quad , \tag{4}$$

where r_0 is the fundamental anisotropy at time = 0. The steady-state fluorescence anisotropy is the normalized average of the time-dependent anisotropy decay *r(t)* weighted by the fluorescence intensity as shown in eq 5

$$r = \frac{\int_0^{\infty} r(t) I(t) dt}{\int_0^{\infty} I(t) dt} \quad . \tag{5}$$

Fluorescence anisotropy decay measurements can resolve the timescales and amplitudes of multiple motions experienced by complex fluorophore-labeled macromolecules, including global

and local motions. The fluorescence anisotropy decay of a sample characterized by multiple rotational motions is defined as

$$r(t) = r_0\left(\sum_i F_i e^{-t/\tau_{c,i}}\right) \ . \quad (6)$$

Time-domain versus frequency-domain anisotropy-decay measurements. As mentioned in the previous section, frequency-domain (FD) measurements involve sample excitation via a continuous monochromatic light source with sinusoidally-modulated intensity.[3] Time-domain (TD) and FD data can be interconverted via Laplace transforms (Figure S2). The direct conversion of raw FD data into raw TD data, however, is unnecessary. Therefore the FD and TD methodologies are of comparable practical convenience.[4] While TD instruments are often more sensitive than FD instruments, FD measurements are typically able to more effectively resolve multi-component anisotropy decays (especially if they encompass a wide temporal regime, e.g. from ps to 50-100 ns) than TD measurements.[3] In this work, we exploited the FD methodology to monitor fluorescence anisotropy decays.

In FD measurements, the sinusoidally-modulated intensity of the excitation light results in sinusoidal variation in the intensity of the emitted light that is offset in phase and amplitude relative to the excitation light. Before performing fluorescence anisotropy measurements, fluorophore lifetimes are determined from the phase shift (ϕ) and modulation (M) of the emitted light, upon exciting the sample with unpolarized light. The modulation M is defined as

$$M = \frac{AC_{EM}/DC_{EM}}{AC_{EX}/DC_{EX}} \ , \quad (7)$$

where AC is the amplitude of the alternating current, DC is the magnitude of the direct current, and the subscripts EX and EM denote the excitation and emission light respectively.[3]

After determining the fluorescence lifetime(s) of the fluorophore, polarized excitation is used to measure the anisotropy decay. For these measurements, the phase-shift difference ($\Delta\phi$) and

modulation ratio (*Y*) are measured for a range of excitation light modulation frequencies. $\Delta\phi$ and *Y* are defined as

$$\Delta\phi = \phi_{\parallel} - \phi_{\perp} \tag{8}$$

$$\mathrm{Y} = \frac{AC_{EM,\perp}}{AC_{EM,\parallel}} \tag{9}$$

$\phi_{\parallel}$ and $\phi_{\perp}$ are the phase shifts of the parallel and perpendicular components of the polarized emission, respectively.[5] Nonlinear least squares fitting of the graphs of $\Delta\phi$ and *Y* versus the modulation frequency (ω) is used to determine the rotational correlation time of the fluorophore.[5] As mentioned above, FD measurements often provide higher resolution of multi-component anisotropy decays than TD measurements. This feature may be contributed by the fact that FD anisotropy measurements entail collecting two independent quantities, $\Delta\phi(\omega)$ and *Y(ω)*, to determine rotational correlation times, while TD anisotropy measurements rely on the assessment of a single parameter, *r(t)*.[6] FD fluorescence anisotropy decay measurements can differentiate the local dynamics of a fluorophore from the rotational motions of the macromolecule to which it is connected. These measurements can resolve up to three rotational motions as long as the timescale for the motions is faster or comparable to the lifetime of the fluorophore, and the different rotational correlation times differ by at least a factor of ca. five.[3]

Multi-component anisotropy decays depend on two parameters, the rotational correlation times and the fractional contributions of the different motions, as described by

$$r(t) = r_0\left(\sum_i F_i e^{-t/\tau_{c,i}}\right) \tag{10}$$

where t is time, F_i is the fractional contribution of each anisotropy decay term, and $\tau_{c,i}$ is the rotational correlation time for each anisotropy decay term.[3] RNCs can show either two or three rotational motions, so their anisotropy decays are described by either eq 11 (two motions) or eq 12 (three motions).

$$\frac{r(t)}{r(0)} = F_s e^{-t/\tau_{c,S}} + F_F e^{-t/\tau_{c,F}} \quad (11)$$

$$\frac{r(t)}{r(0)} = F_s e^{-t/\tau_{c,S}} + F_I e^{-t/\tau_{c,I}} + F_F e^{-t/\tau_{c,F}} \quad , \quad (12)$$

where F_s, F_I, and F_F are the fractional contribution to the anisotropy decay from the slow, intermediate, and fast rotational motions, respectively.[3] $\tau_{c,S}$, $\tau_{c,I}$, and $\tau_{c,F}$ denote the rotational correlation times for the slow, intermediate, and fast motions. Figure 5a shows simulated anisotropy decay data for RNCs with 2 and 3 rotational motions. RNCs with three rotational motions show an increase in the phase shift difference at intermediate modulation frequencies, resulting in a "bump" in the phase change data. The "bump" spectral feature indicates the presence of motions on the ns timescale.[3] In order to determine whether a sample shows two or three rotational motions, the anisotropy decay data is fit with both a two-component and a three-component exponential decay and the χ^2 values for both fits are compared. The three-component fit must have a χ^2 value at least 2.5-fold smaller than the χ^2 value for the two-component fit for the presence of three rotational motions to be confirmed.[3]

Determination of reduced χ^2 values. In order to determine whether the fluorescence anisotropy decay data fit best to a two- or three-component model, reduced χ^2 values resulting from fits to both models (evaluated independently) were computed. Reduced χ^2 values show how well curve fits match experimental results. The following equation was used to determine reduced χ^2 values

$$\chi^2 = \frac{1}{2n-f-1}\sum_{\omega}\left(\frac{\Delta\phi_\omega - \Delta\phi_{c\omega}}{\delta\Delta\phi}\right)^2 + \frac{1}{2n-f-1}\sum_{\omega}\left(\frac{Y_\omega - Y_{c\omega}}{\delta Y}\right)^2 \quad , \quad (13)$$

where n is the number of experimental light intensity modulation frequencies, f is the number of free-floating parameters used in the least-squares analysis, $\Delta\phi_\omega$ and $\Delta\phi_{c\omega}$ denote the experimental and calculated phase shift difference, Y_ω and $Y_{c\omega}$ are the experimental and

calculated modulation ratios, and $\delta\Delta\phi$ and δY are the uncertainties in the phase shift difference and modulation ratio.[3, 7] The last two parameters were set to 0.2° and 0.004, respectively.[3, 5] Lowest possible reduced χ^2 values (< 5) are desirable. If χ^2 decreased by a factor of >2.5 for the three-component fit relative to the two-component fit, the three-component fit was determined to be the best fit for the data, consistent analogous criteria employed in the literature.[3, 8]

RNC populations that may be interacting with ribosomal surface (or chaperones) are in slow exchange on the fluorescence-lifetime timescale. As schematically illustrated in Figure S4, it is in principle possible that any nascent-chain interactions with the ribosomal surface may affect observed fluorescence-anisotropy decay parameters. In order to test whether this is true, we started by estimating the diffusion-limited association rate constant and matching timescales for interactions between the nascent protein and the ribosome. The goal of this section is to use kinetic arguments to show that RNC populations that interact or do not interact with the ribosome (and molecular chaperones) are in slow exchange on the fluorescence-lifetime timescale. The next section goes on to prove that, under slow-exchange conditions, experimental rotational correlation times for intermediate-timescale ns motions are not affected by the presence of nascent-chain interactions with the ribosomal surface.

We modeled the fastest possible interactions of nascent chains with the ribosomal surface as diffusion-limited intramolecular collisions of small particles (i.e., compact nascent chains) towards larger tethered particles (i.e., the ribosome). In general, for the diffusion of particles toward an "absorbing sphere", the number of collisions per second, or current (*I(r)*, in units s^{-1}), is equal to the number of particles colliding per unit area per second (flux, *J(r)*) multiplied by the sphere's surface area, as shown below[9]

$$I(r) = J(r)4\pi r^2 = -4\pi D c_\infty r \ , \qquad (14)$$

where D is the translational diffusion coefficient of the nascent chain and r is the radius of the ribosome (114.1 Å, determined from Pymol measurements of PDB: 4ybb). The association rate is described by the rate constant $k_{assoc.}$, which denotes the frequency of collisions through the solution volume per molecule, in units of cm^3s^{-1}. Now, $k_{assoc.}$ for a diffusion-limited process can be estimated via the relation

$$k_{assoc.} = 4\pi Dr \quad , \tag{15}$$

and the association lifetime ($t_{assoc.}$), corresponding to the average time between collisions, can be determined by dividing the volume sampled by the tethered particle (V) by the rate constant

$$t_{assoc.} = \frac{V}{k_{assoc.}} \quad . \tag{16}$$

Eqs 15-16 were used to estimate the association lifetime ($t_{assoc.}$) for the interaction between nascent chain and ribosome. For this system, $t_{assoc.}$ is equal to the average time between collisions between the ribosome and the nascent protein. D was estimated via the Stokes-Einstein equation (eq 11 in main text) with radius = 16.1 Å (determined from Pymol measurements of PDB: 1mbc), viscosity = 1.08 mPa-s, and temperature = 298 K. The range of values for the volume (V) available for nascent-chain local diffusion was estimated from two limiting cases. Namely, *model a*, which assumes that the compact RNC region is located within the ribosomal vestibule (Figure S5a), and *model b*, which assumes that the nascent chain lies on the outer surface of the ribosome (Figure S5b). For *model a,* the volume of the vestibule was estimated as $1/5^{th}$ of the total ribosomal tunnel volume giving an approximate volume of 7.7 nm^3 (total tunnel volume = 38.5 nm^3, Figure S5a).[10] In *model b*, the smallest diffusion volume was estimated from a cone with a height of 56 Å and a semi-angle of 15° (experimental value of cone semi-angle) yielding a volume of ~13.2 nm^3 (Figure S5b). The cone height in *model b* was chosen to accommodate the expected size of the RNC globular domain (assuming spherical shape) within a cone bearing an

apex angle of 30° (i.e., twice the experimental cone semi-angle). Using the above volume estimates, the estimated $t_{assoc.}$ was estimated to be 0.4 – 0.7 ns. The diffusion volumes and $t_{assoc.}$ values for these models are summarized in Table S2. The limiting estimates in Table S2 refer to the smallest possible diffusion volumes, yielding the fastest possible association rate constants. Therefore, the actual association rate is likely slower than these estimates. Even considering this worst-case scenario, the shortest possible association lifetime (0.4 – 0.7 ns) is of similar order of magnitude to the fluorescence lifetime of the fluorophore BODIPY-FL.[8] Therefore, if interactions between the nascent chain and ribosome occur, they are expected not to be fully averaged relative to the timescale of the fluorescence lifetime of the BODIPY-FL label. Note that the fluorescence lifetime establishes the relevant timescale of anisotropy decay measurements, given the definition of fluorescence anisotropy.

In summary, compact independently tumbling nascent chains are expected to be in slow exchange with any ribosome-bound (or large-chaperone-bound) conformations, on the fluorescence anisotropy-decay timescale.

Derivation of anisotropy-decay equation for mixture of multiple RNC populations. Given that any potential interactions between nascent chain and the ribosome are in slow exchange relative to the fluorescent lifetime of the fluorophore, we considered how a mixture of multiple RNC populations may affect experimentally observed anisotropy decay parameters. Here, we show the derivation of the anisotropy decay equation for a mixture of two species: RNCs that tumble independently from the ribosome and RNCs that interact with the ribosome (Figure S4). The non-interacting species has three rotational correlation times (slow, intermediate, and fast timescales) and is labeled contributing (C) because it contributes to the intermediate-timescale rotational correlation time. The interacting species has two rotational correlation times (slow and

fast timescales) and is labeled noncontributing (NC). If both species are labeled with the same fluorophore and the fluorophores experience the same environment, then the observed anisotropy decay for the mixture is a sum of their anisotropy decays multiplied by the mole fraction of each species, as shown in eq 17 (see eq 11 in Knight *et al.* supporting information[11])

$$r_{obs}(t) = \sum_i r_{0,i} x_i r_i(t) \quad . \tag{17}$$

Both species have the same r_0 value because they have the same fluorophore, so eq 17 becomes

$$\frac{r_{obs(t)}}{r_0} = x_C r_C(t) + x_{NC} r_{NC}(t) \tag{18}$$

where x_C and x_{NC} are the mole fractions for the contributing and noncontributing species. The anisotropy decay values $r_C(t)$ and $r_{NC}(t)$ are defined as[12]

$$\frac{r_C(t)}{r_0} = \left(1 - S_{F,C}^2\right) e^{\left(\frac{-t}{\tau_{c,F}}\right)} + S_{F,C}^2 \left(1 - S_{I,C}^2\right) e^{\left(\frac{-t}{\tau_{c,I}}\right)} + S_{I,C}^2 S_{F,C}^2 e^{\left(\frac{-t}{\tau_{c,S}}\right)} \tag{19}$$

and

$$\frac{r_{NC}(t)}{r_0} = \left(1 - S_{F,NC}^2\right) e^{\left(\frac{-t}{\tau_{c,F}}\right)} + S_{F,NC}^2 e^{\left(\frac{-t}{\tau_{c,S}}\right)} \quad . \tag{20}$$

In addition, the following constraints are applied. First, both free and bound nascent-chains have rotational correlation times for the slow motions (corresponding to the global tumbling of ribosomal complexes) set to the same nominal limiting value of 1 μs. Second, the fast local motions of the nascent-chain N terminus have very similar experimental rotational correlation times (0.1-0.3 ns) under conditions where a different extent of interactions are expected (i.e., in the absence and presence of molecular chaperones). Therefore, rotational correlation times for the fast motions are assumed to be the same for free and bound species. Under the above conditions, eqs 19 and 20 can be substituted into eq 18 to yield

$$\frac{r_{obs}(t)}{r_0} = x_C \left[\left(1 - S_{F,C}^2\right) e^{\left(\frac{-t}{\tau_{c,F}}\right)} + S_{F,C}^2 \left(1 - S_{I,C}^2\right) e^{\left(\frac{-t}{\tau_{c,I}}\right)} + S_{I,C}^2 S_{F,C}^2 e^{\left(\frac{-t}{\tau_{c,S}}\right)} \right] +$$

$$x_{NC}\left[\left(1-S_{F,NC}^{2}\right)e^{\left(\frac{-t}{\tau_{c,F}}\right)}+\ S_{F,NC}^{2}e^{\left(\frac{-t}{\tau_{c,S}}\right)}\right]\ . \tag{21}$$

The latter expression can be simplified to yield eq 22

$$\frac{r_{obs}(t)}{r_0}=\left[x_C\left(1-S_{F,C}^{2}\right)+x_{NC}\left(1-S_{F,C}^{2}\right)\right]e^{\left(\frac{-t}{\tau_{c,F}}\right)}+x_C S_{F,C}^{2}\left(1-S_{I,C}^{2}\right)e^{\left(\frac{-t}{\tau_{c,I}}\right)}+$$

$$\left(x_C S_{I,C}^{2}S_{F,C}^{2}+x_{NC}S_{F,NC}^{2}\right)e^{\left(\frac{-t}{\tau_{c,S}}\right)}\ . \tag{22}$$

Importantly, eq 22 demonstrates that the presence of ribosome-associated populations (interacting species) does not lead to any changes in rotational correlation time.

On the other hand, the presence of an interacting species does lead to changes in observed order parameters. The order parameters for a mixture can be determined from the fractional anisotropy decay intensities via eqs 23-26 as follows[12]

$$f_{S,obs}=\left(x_C S_{I,C}^{2}S_{F,C}^{2}+\ x_{NC}S_{F,NC}^{2}\right)\quad , \tag{23}$$

$$f_{I,obs}=\ x_C S_{F,C}^{2}\left(1-S_{I,C}^{2}\right)\ , \tag{24}$$

$$f_{F,obs}=\ x_C\left(1-S_{F,C}^{2}\right)+x_{NC}\left(1-S_{F,C}^{2}\right)\ , \tag{25}$$

$$x_C+x_{NC}=1\ . \tag{26}$$

Eqs 23-26 can be solved upon assuming that the S^2 values for the fast motions are the same for free and bound species. This assumption is reasonable because it was experimentally found that the fluorescent dye has no affinity for the ribosome.[12] The order parameters and cone semi-angles for a range of mole fraction values for the independently tumbling (contributing) species are shown in Table S3. This table shows that even if the independently tumbling population is very small (i.e., 0.2), the cone-semi angle for the intermediate timescale motions is at most 39º. This value is significantly smaller than the maximum value of 180º. This small cone semi-angle

illustrates the fact that, regardless of any ribosome (or chaperone) interactions with the nascent protein, nascent chain motions are highly spatially confined.

Oligonucleotide sequences used in cell-free reaction. In order to create stalled ribosome-nascent chain complexes, cell-free expression of full-length apoMb ($apoMb_{153}$) was performed in the presence of oligodeoxynucleotides bearing a sequence complementary to the sequence of the desired mRNA region to be subsequently cleaved by the endogenous *E. coli* RNAse H enzyme.[13] The target mRNA region was designed to "hide" the apoMb gene stop codon, to generate RNCs of full-length apoMb. In addition, an anti-SSRA oligonucleotide was added to the cell-free reaction to prevent tmRNA-mediated release of the nascent chain from the stalled ribosome.[14] The final cell-free concentration of the above oligonucleotides was 0.15 μg/μL. The sequences of the oligonucleotides are

5'- ACCCTGGTAACCCAGTTCTTTGTACTTAGCAGCGATAT-3', full-length ApoMb RNC sequence, and

5'- TTAAGCTGCTAAAGCGTAGTTTTCGTCGTTTGCGACTA-3', anti-ssrA oligonucleotide.

SUPPORTING FIGURES

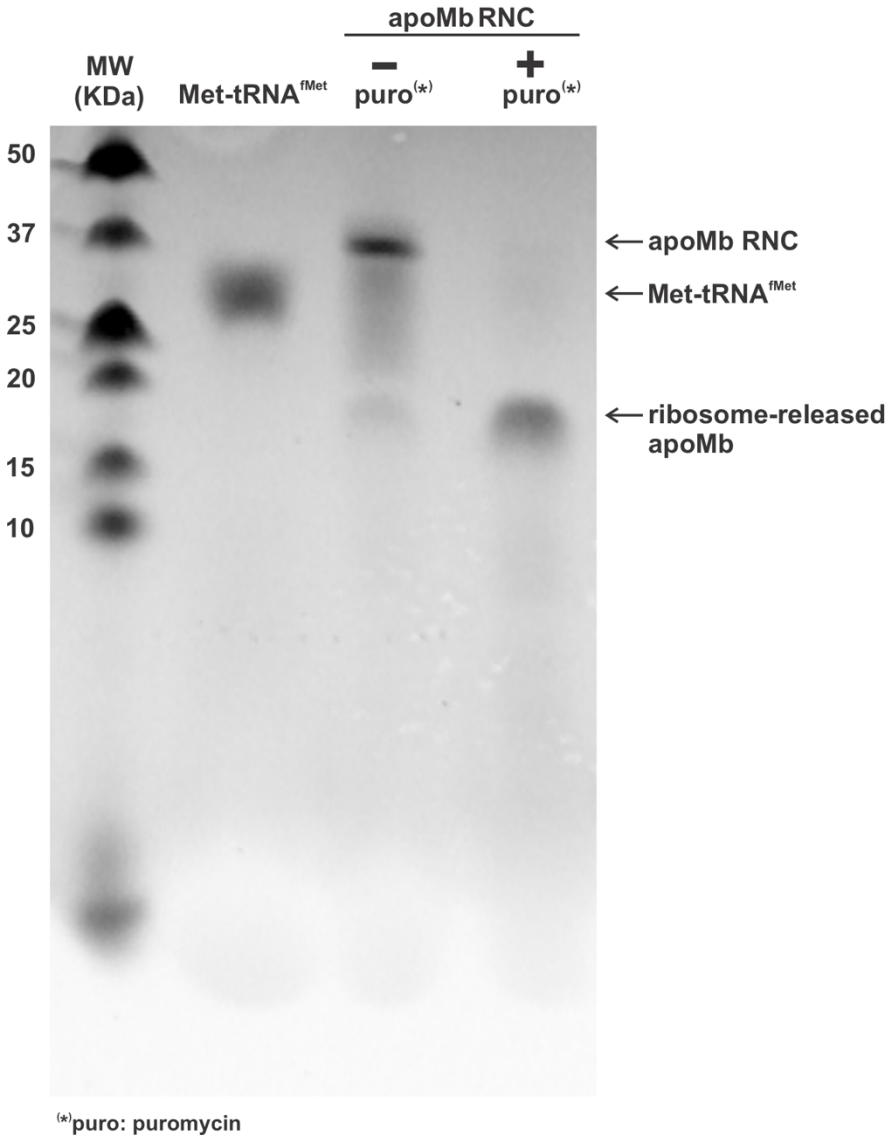

Figure S1. Representative gel illustrating a typical puromycin assay performed on RNCs of full-length apoMb (apoMb$_{153}$). Bands are visualized via in-gel fluorescence. The shift to lower molecular weight upon addition of the puromycin (puro) antibiotic proves that the nascent chain was ribosome-bound (therefore an actual RNC) prior to treatment with puro. Met-tRNA^{fMet} and apoMb RNCs are site-specifically labeled with BODIPY-FL at the N terminus.

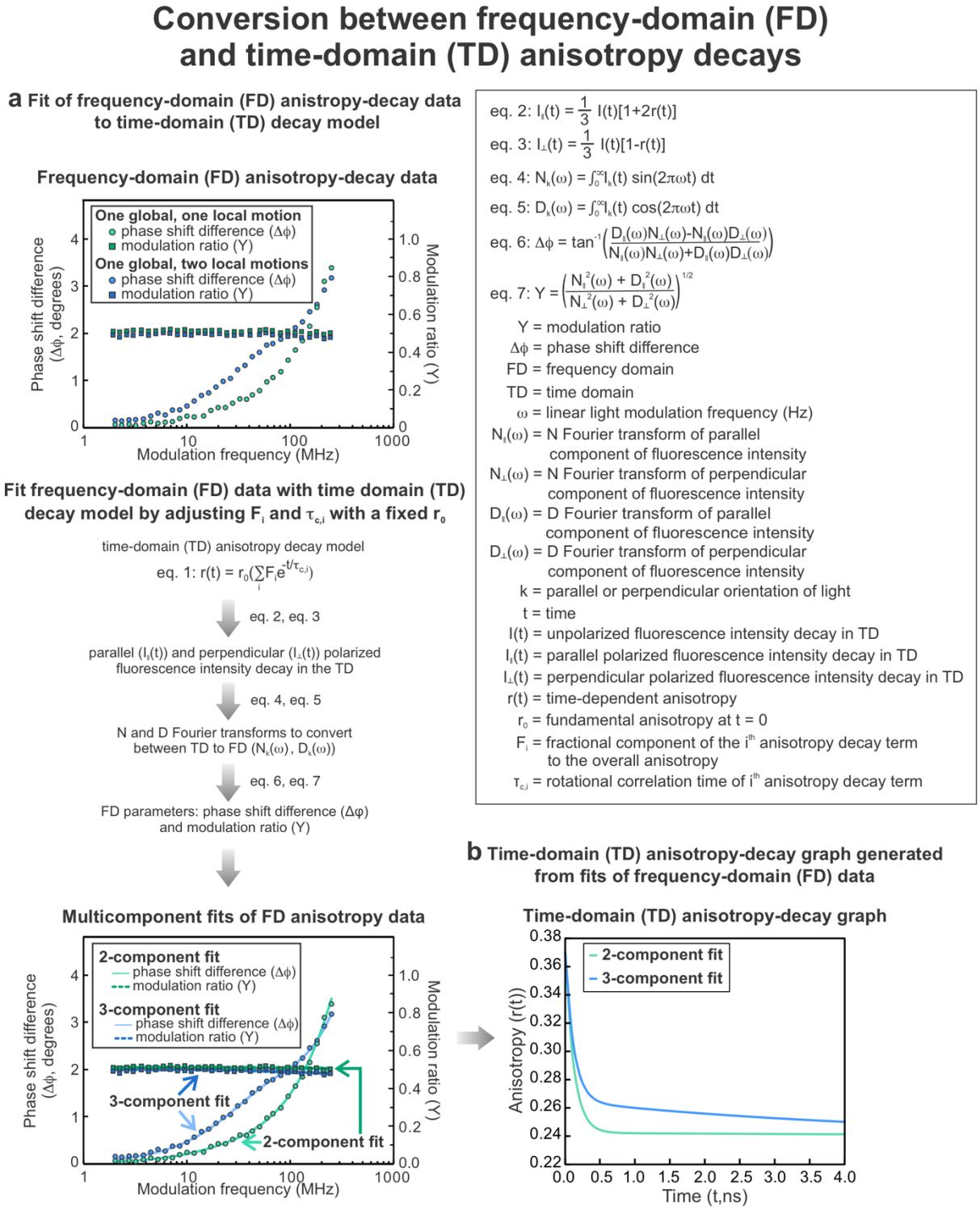

Figure S2. (a) Procedure employed to fit FD anisotropy-decay data to time-domain anisotropy decay models. (b) TD anisotropy-decay graph generated from fits of FD data.

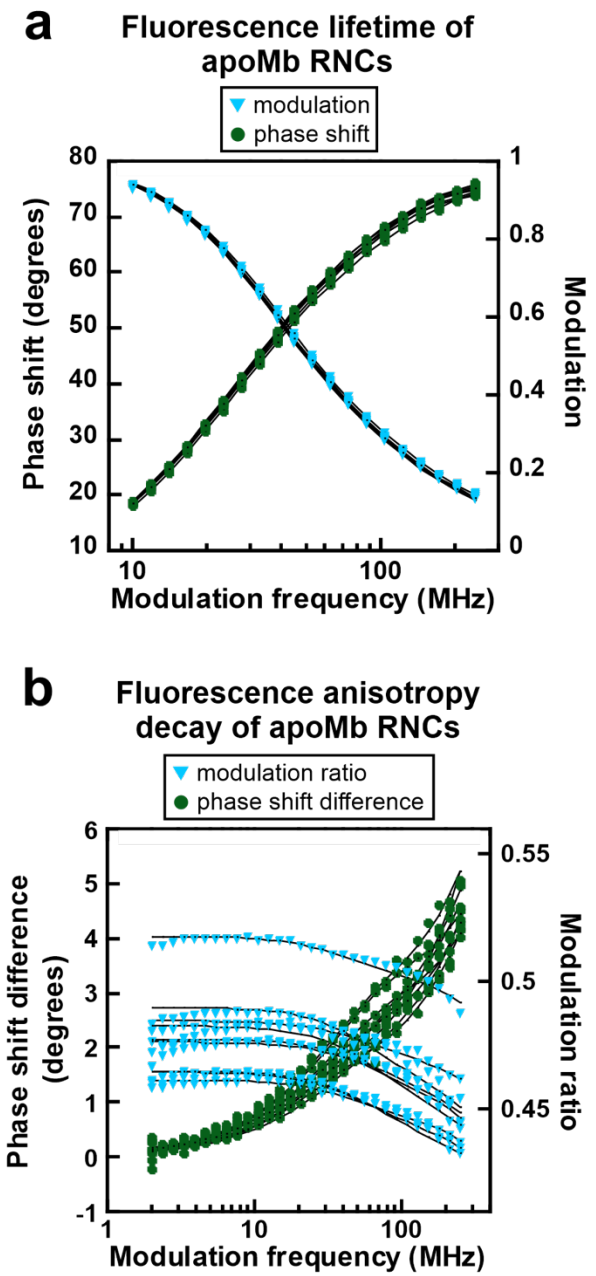

Figure S3. (a) Fluorescence lifetime and (b) anisotropy-decay graphs for all the data collected in this work.

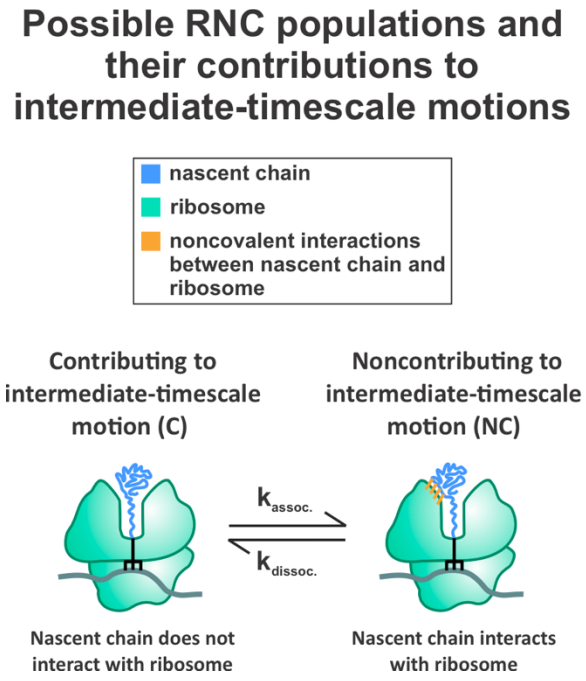

Figure S4. Simplified models illustrating RNC conformations consistent with the data collected in this work. RNCs that do not interact with the ribosome show a three-component anisotropy decay and contribute to the intermediate timescale motion (C). RNCs that interact with the ribosome show a two-component anisotropy decay and do not contribute to the intermediate-timescale motion (NC).

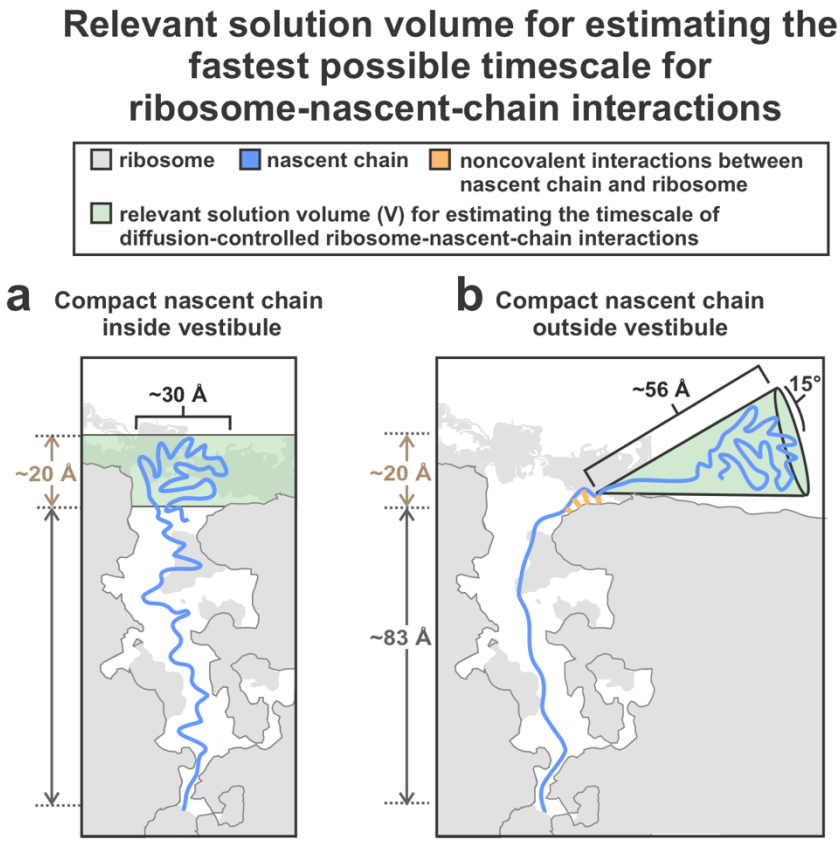

Figure S5. Limiting models employed to estimate relevant solution volumes (V) for diffusion-controlled association of nascent chains with ribosomal surface. (a) Model assuming that the compact nascent chain-region is contained within the ribosomal vestibule. (c) Model assuming that the compact nascent chain-region is outside of the ribosomal vestibule. Diffusion volumes estimated from the experimental cone semi-angle of 15°. Green regions indicate relevant solution volumes for the hypothetical diffusion-controlled association between the nascent chain and the ribosome. Ribosome dimensions were estimated from Dao Duc *et al.*[10]

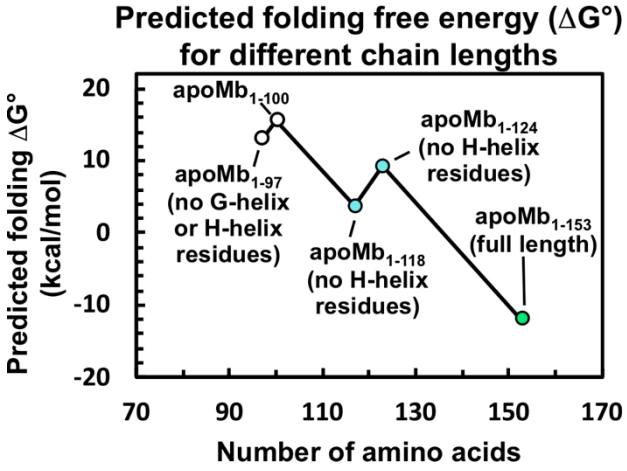

Figure S6. Predicted folding free energy of apoMb N-terminal fragments of increasing length, assuming a native-like conformation. This plot is a complement to the main-article Figure 12. Additional chain lengths ($apoMb_{1\text{-}100}$ and $apoMb_{1\text{-}118}$) are included here, to show the predicted thermodynamic contribution of loop regions between helices. $ApoMb_{1\text{-}100}$ includes the unstructured region between helices F and G. $ApoMb_{1\text{-}124}$ includes the unstructured region between helices G and H. All free energy calculations were carried out with FoldX version 5.[15] PDB files for apoMb (RCSB PDB: 1mbc) were generated with Pymol version 2.0.0.

SUPPORTING TABLES

Table S1. Statistical p values for the viscosities of the apoMb$_{153}$ RNC solution measured at shear rates ranging from 1500 s^{-1} to 8000 s^{-1} shown in Figure 4. P values were determined from a two-tailed Student's test assuming unequal variances. P values > 0.05 indicate data that are not statistically different (orange).

		Shear rate (s^{-1})				
		1,500	3,000	5,000	6,500	8,000
Shear rate (s^{-1})	1,500	–	0.58	0.29	0.27	0.37
	3,000		–	0.98	0.70	0.28
	5,000			–	0.56	0.28
	6,500				–	0.23
	8,000					–

Table S2. Statistical p values comparing the viscosities of the apoMb$_{153}$ RNC solution and buffer system lacking RNCs measured at shear rates ranging from 1500 s^{-1} to 8000 s^{-1} shown in Figure 4. P values were determined from a two-tailed Student's test assuming unequal variances. P values > 0.05 indicate data that are not statistically different (orange).

Shear rate (s^{-1})	apoMb$_{153}$ RNC solution vs buffer system without RNCs
1,500	0.40
3,000	0.93
5,000	0.62
6,500	0.35
8,000	0.14

Table S3. Estimates of relevant solution volume for estimating fastest possible timescale for ribosome-nascent-chain interactions as shown in Figure S5

Model	Diffusion volume (nm^3)[a]	$t_{assoc.}$ (ns)
Compact subdomain contained in vestibule (Figure S5b)	7.7	0.43
Compact subdomain outside vestibule. Volume is a cone with semi-angle of 15° (Figure S5c)	13.2	0.73

a. Diffusion volume is the relevant solution volume for association between the nascent chain and the ribosome.

Table S4. Intermediate-timescale motion cone semi-angles and order parameter values for different mole fractions of contributing species

Mole fraction of contributing species (x_C)	S_I^2	S_I	Cone semi-angle (θ_I, deg)
0.1	-0.03 ± 0.09	(Cannot calculate from negative S_I^2)	(Cannot calculate from negative S_I^2)
0.2	0.48 ± 0.04	0.70 ± 0.06	39 ± 2
0.3	0.66 ± 0.03	0.81 ± 0.04	30 ± 2
0.4	0.74 ± 0.02	0.86 ± 0.03	25 ± 1
0.5	0.79 ± 0.02	0.89 ± 0.02	22 ± 1
0.6	0.83 ± 0.01	0.91 ± 0.02	20.0 ± 0.9
0.7	0.85 ± 0.01	0.92 ± 0.01	18.4 ± 0.8
0.8	0.87 ± 0.01	0.93 ± 0.01	17.2 ± 0.8
0.9	0.89 ± 0.01	0.94 ± 0.01	16.1 ± 0.7
1	0.897 ± 0.005	0.947 ± 0.005	15.3 ± 0.7

SUPPORTING REFERENCES

1. Odom, O. W.; Hardesty, B. Use of 50 S-binding antibiotics to characterize the ribosomal site to which peptidyl-tRNA is bound. *J. Biol. Chem.* **1992,** *267*, 19117-19122.
2. Ziehr, D. R.; Ellis, J. P.; Culviner, P. H.; Cavagnero, S. Production of ribosome-released nascent proteins with optimal physical properties. *Anal. Chem.* **2010,** *82*, 4637-4643.
3. Weinreis, S. A.; Ellis, J. P.; Cavagnero, S. Dynamic fluorescence depolarization: A powerful tool to explore protein folding on the ribosome. *Methods* **2010,** *52*, 57-73.
4. Jameson, D. M.; Gratton, E.; Hall, R. D. The measurement and analysis of heterogeneous emissions by multifrequency phase and modulation fluorometry. *Appl. Spectrosc. Rev.* **1984,** *20*, 55-106.
5. Ross, J. A.; Jameson, D. M. Time-resolved methods in biophysics. 8. Frequency domain fluorometry: applications to intrinsic protein fluorescence. *Photochem. Photobiol. Sci.* **2008,** *7*, 1301-1312.
6. Lakowicz, J. R. *Principles of Fluorescence Spectroscopy*. 3rd ed.; New York : Plenum Press: 2006.
7. Lakowicz, J. R.; Laczko, G.; Cherek, H.; Gratton, E.; Limkeman, M. Analysis of fluorescence decay kinetics from variable-frequency phase shift and modulation data. *Biophys. J* **1984,** *46*, 463-477.
8. Ellis, J. P.; Bakke, C. K.; Kirchdoerfer, R. N.; Jungbauer, L. M.; Cavagnero, S. Chain dynamics of nascent polypeptides emerging from the ribosome. *ACS Chem. Biol.* **2008,** *3*, 555-566.
9. Dill, K. A. *Molecular Driving Forces: Statistical Thermodynamics in Chemistry and Biology*. 2nd ed.; New York : Garland Science: 2011.
10. Dao Duc, K.; Batra, S. S.; Bhattacharya, N.; Cate, Jamie H. D.; Song, Yun S. Differences in the path to exit the ribosome across the three domains of life. *Nucleic Acids Res.* **2019,** *47*, 4198-4210.
11. Knight, A. M.; Culviner, P. H.; Kurt-Yilmaz, N.; Zou, T.; Ozkan, S. B.; Cavagnero, S. Electrostatic effect of the ribosomal surface on nascent polypeptide dynamics. *ACS Chem. Biol.* **2013,** *8*, 1195-1204.
12. Ellis, J. P.; Culviner, P. H.; Cavagnero, S. Confined dynamics of a ribosome-bound nascent globin: Cone angle analysis of fluorescence depolarization decays in the presence of two local motions. *Protein Sci.* **2009,** *18*, 2003-2015.
13. Behrmann, M.; Koch, H. G.; Hengelage, T.; Wieseler, B.; Hoffschulte, H. K.; Müller, M. Requirements for the translocation of elongation-arrested, ribosome-associated OmpA across the plasma membrane of Escherichia coli. *J. Biol. Chem.* **1998,** *273*, 13898-13904.
14. Hanes, J.; Plückthun, A. In vitro selection and evolution of functional proteins by using ribosome display. *Proc. Natl. Acad. Sci. U. S. A.* **1997,** *94*, 4937-4942.
15. Schymkowitz, J.; Borg, J.; Stricher, F.; Nys, R.; Rousseau, F.; Serrano, L. The FoldX web server: an online force field. *Nucleic Acids Res.* **2005,** *33*, W382-W388.